Wave propagation and wavefield reconstruction in viscoelastic media

Tieyuan Zhu, Jackson School of Geosciences, the University of Texas at Austin

SUMMARY

This paper presents wave propagation and wavefield reconstruction in viscoelastic media. In terms of the decoupled attenuation property of the viscoelastic wave equation, wave propagation can be simulated with three scenarios: only amplitude loss effect, only phase dispersion effect, and both, which brings convenience and options for users. For example, it benefits to seismic imaging problem. Wavefield reconstruction can be completed simply by reversing the sign of both the P- and S-wave loss operators. Attenuation effects are thus compensated for during back-propagation wave propagation. I demonstrate the advantages of the decoupled attenuation property in the context of wave propagation and wavefield reconstruction using several numerical examples.

INTRODUCTION

Seismic wave propagation has anelastic characteristics in real Earth materials. Particularly, in exploration geophysics the target area (the hydrocarbon reservoir) shows high seismic attenuation (i.e., low quality factor, Q) which may be caused by the presence of overpressured free gas accumulations (e.g., Carcione et al. 2003; Dvorkin and Mavko 2006). As a result, the recorded signals are significantly affected in amplitude and phase. Therefore, an accurate wavefield modeling approach should be able to account for the effects of attenuation and velocity dispersion.

In the field of seismology, there have two category approaches for viscoelastic simulations. One is based on the generalized Zener model and memory variables to model anelastic wave propagation (e.g., Carcione et al. 1988). The second approach is based on constant-Q given by Kjartansson (1979). This model has been shown to describe the behavior of seismic waves in Pierre shale (McDonal et al., 1958). The model involves a fractional time derivative, i.e. an irrational (or non-integer) degree of the time derivative (Caputo and Mainardi, 1971). The Grnwald-Letnikov approximation (Podlubny, 1999) is used to compute this time derivative (Carcione et al., 2002; Carcione, 2009). However, this formulation is based on the history of the wavefield, thus requiring to store in memory all the previous values to present time. It becomes unaffordable for practical seismic modeling studies, in particular for three-dimensional simulations, even though it is possible to truncate the fractional operator after a given time period (Carcione et al., 2002).

To avoid the memory requirements of the fractional time operators, Zhu and Carcione (2014)rather derived viscoelastic wave equation using fractional space derivatives. This operation, computed with the fractional Fourier pseudospectral method, avoids the storage of wavefields, rendering the modeling as efficient as the simulation in lossless media.

In this paper, I further illustrate the decoupling P- and S-wave attenuation property with the analysis of separated two operators in the viscoelastic wave equation (Zhu and Carcione, 2014). I found that the first-derivative terms in the wave equation correspond to P- and S-wave amplitude loss and the rest operators of the right-hand side correspond to dispersion. it using numerical simulations in a homogeneous model. To make it available for seismic imaging, I design a viscoelastic back-propagation approach that can correct for both P- and S-attenuation effects. In terms of this property, a viscoelastic back propagation modeling equation is formulated by reversing the sign of both P- and S-attenuation operators. I demonstrate these features of the viscoelastic back-propagation approach with two synthetic models.

VISCOELASTIC WAVE PROPAGATION

The frequency-independent Q model (i.e., constant-Q model) is considered to be a practical approximate Q model for exploration seismology problems. Based on the mathematical constant-Q model (Kjartansson, 1979), the 2-D velocity-stress formulation of the viscoelastic wave equation is given by (Zhu and Carcione, 2014)

$$\begin{aligned}
\rho\partial_t v_1 &= (\partial_1\sigma_{11}+\partial_3\sigma_{13}+f_1), && (1)\\
\rho\partial_t v_3 &= (\partial_1\sigma_{13}+\partial_3\sigma_{33}+f_3), && (2)\\
\sigma_{11} &= \left[\eta_p B_p(\varepsilon_{11}+\varepsilon_{33})-2\eta_s B_s\varepsilon_{33}\right] \\
&+ \left[\tau_p A_p\partial_t(\varepsilon_{11}+\varepsilon_{33})-2\tau_s A_s\partial_t\varepsilon_{33}\right], && (3)\\
\sigma_{33} &= \left[\eta_p B_p(\varepsilon_{11}+\varepsilon_{33})-2\eta_s B_s\varepsilon_{11}\right] \\
&+ \left[\tau_p A_p\partial_t(\varepsilon_{11}+\varepsilon_{33})-2\tau_s A_s\partial_t\varepsilon_{11}\right], && (4)\\
\sigma_{13} &= \left[2\eta_s B_s\varepsilon_{13}+2\tau_s A_s\partial_t\varepsilon_{13}\right], && (5)\\
\varepsilon_{11} &= \partial_1 u_1, \varepsilon_{33}=\partial_3 u_3, \varepsilon_{13}=\frac{1}{2}(\partial_3 u_1+\partial_1 u_3), && (6)
\end{aligned}$$

where ρ is the mass density. v_i, σ_i, ε_{ij}, and f_i denote the particle velocity tensor, the stress tensor, the strain tensor and body force components, respectively. u_i is the displacement and $v_i=\partial_t u_i$. i,j are spatial indices. Einsteins convention of repeated indices is assumed. And,

$$A_{P,S}=(-\Delta)^{\gamma_{P,S}-1/2}, B_{P,S}=(-\Delta)^{\gamma_{P,S}}, \quad (7)$$

where

$$\begin{aligned}
\tau_P &= C_\lambda c_{P0}^{2\gamma_P-1} sin(\pi\gamma_P), & \eta_P &= C_\lambda c_{P0}^{2\gamma_P} cos(\pi\gamma_P),\\
\tau_S &= C_\mu c_{S0}^{2\gamma_S-1} sin(\pi\gamma_S), & \eta_S &= C_\mu c_{S0}^{2\gamma_S} cos(\pi\gamma_S),\\
C_\lambda &= M_0\omega_0^{-2\gamma_P}, & C_\mu &= \mu_0\omega_0^{-2\gamma_S}, \qquad (8)
\end{aligned}$$

and ω_0 is an arbitrary reference frequency, which should be higher than the source frequencies to guarantee pulse delay with respect to the lossless case. Also, $\gamma_{p,s}=atan(Q_{p,s}^{-1})/\pi$, and $0<\gamma_{p,s}<0.5$ for any positive value of Q, where Q_p and Q_s are the P- and S-wave quality factors, respectively.

The P-wave modulus M_0 and the S-wave modulus μ_0 are respectively given by $M_0 = \rho c_{p0}^2 cos^2(atan(Q_p^{-1})/2)$ and $\mu_0 = \rho c_{s0}^2 cos^2(atan(Q_s^{-1})/2)$, and c_{p0} and c_{s0} are the P- and S-wave velocities at the reference frequency, respectively.

To solve the wave equation in inhomogeneous media, I use the staggered-grid finite-difference approach to discretize the time derivatives and the staggered-grid pseudospectral approach to discretize the first-order spatial derivatives. The fractional Laplacian operators are solved by the fractional Fourier pseudospectral method as shown by (Zhu and Harris, 2014).

Note that the first-order time-derivative terms in equations 3, 4, and 5 correspond to attenuation-associated P- and S-wave loss operators. When $Q_{p,s} \to \infty$ ($\gamma_{p,s} \to 0$), the first-order time-derivative terms disappear, and equations **??** only contain second-order time derivatives, and becomes an elastic wave equation.

To demonstrate decoupled amplitude loss and velocity dispersion for both P- and S-waves, I set up a homogeneous model with a vertical force source in the origin. $Q_p = 30$ and $Q_s = 15$. Figure 1a shows the snapshot of the elastic simulation with $Q_{p,s} \to \infty$. The wavefront is labeled by the red dashed line. Figure 1d shows the viscoelastic simulation using equations 1-5 (smaller amplitude and phase delay). Figure 1b shows the amplitude-loss simulation (only smaller amplitude, no phase delay). Figure 1c shows the dispersion simulation (only phase delay, no loss).

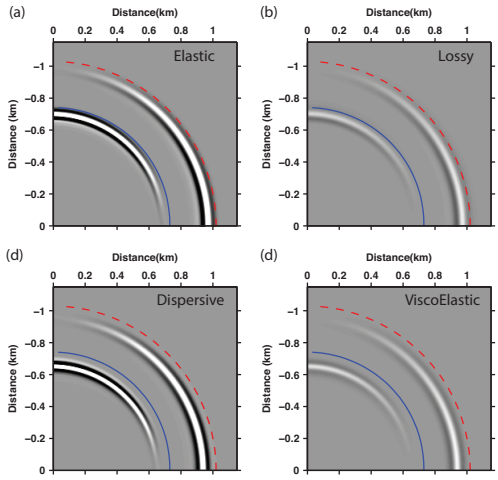

Figure 1: Wavefield snapshots using (a)elastic; (b) amplitude-loss; (c) dispersive; (a)viscoelastic;

VISCOELASTIC WAVEFIELD RECONSTRUCTION

To implement back propagation in the time-domain wave equation mathematically, I first replace time t by t. Due to attenuation during forward propagation, I have to amplify amplitude during the propagation of the time-reversed wavefields. The amplification of amplitude is done by reversing the sign of the P-wave loss operator (Zhu, 2014). For the viscoelastic case, I reverse the sign of both P- and S-wave loss operators. Assuming $\hat{t} = -t$, the viscoelastic TR modeling equations with attenuation compensation are written as

$$\begin{aligned}
\sigma_{11} &= \left[\eta_p B_p(\varepsilon_{11}+\varepsilon_{33}) - 2\eta_s B_s \varepsilon_{33}\right], \\
&- \left[\tau_p A_p \partial_t(\varepsilon_{11}+\varepsilon_{33}) - 2\tau_s A_s \partial_t \varepsilon_{33}\right], \qquad (9)\\
\sigma_{33} &= \left[\eta_p B_p(\varepsilon_{11}+\varepsilon_{33}) - 2\eta_s B_s \varepsilon_{11}\right], \\
&- \left[\tau_p A_p \partial_t(\varepsilon_{11}+\varepsilon_{33}) - 2\tau_s A_s \partial_t \varepsilon_{11}\right], \qquad (10)\\
\sigma_{13} &= 2\eta_s B_s \varepsilon_{13} - 2\tau_s A_s \partial_t \varepsilon_{13}, \qquad (11)
\end{aligned}$$

Substituting equations 9, 10,and 11 into equation 1 and 2 (with $\hat{t} = -t$), we can see that the solution $v(\mathbf{x}, -t)$ of equations 1, 2, 9, 10,and 11 is the time-reversed version of the solution $v(\mathbf{x}, t)$ of the forward modeling equations (1, 2, 3, 4, and 5), where $\mathbf{x} = (x, y, z)$. Simply, the waveform at a forward time t is physically equivalent to that at the reversed time $-t$. Therefore, the above system for time-reverse modeling becomes time-invariant.

For the reverse modeling, the input data consists of two particle velocity components (vertical and horizontal). No body force is present throughout the time-reversal propagation, i.e.,$f_i = 0$. The recorded particle velocity components are reversed in time and enforced as the Dirichlet boundary condition at receivers; mathematically they are expressed as

$$v_1(\mathbf{x}_r, -t) = v_x(T-t), \qquad (12)$$
$$v_3(\mathbf{x}_r, t) = v_z(T-t) \qquad (13)$$

Here v_x and v_z are the recorded horizontal and vertical particle velocity components at the receivers. T is the total recorded time. The receiver location coordinate in 2-D is $\mathbf{x}_r = (x_r, z_r)$. In practice, the higher frequencies in the recorded data are invariably contaminated with noise. Attenuation compensation during back propagation will amplify such unwanted frequency content. To prevent high-frequency noise from growing exponentially, I apply a low-pass filter in the spatial frequency domain to the right-hand-side attenuation-associated loss and dispersion operators in equations 9, 10, and 11 when calculating the back-propagated wavefields. The filter should not be applied to the propagation operators (Zhu, 2015).

SYNTHETIC EXAMPLES

Wavefield reconstruction by viscoelastic TR

The first example is a 2D homogeneous model. The P-wave velocity is 2500 m/s, the S-wave velocity is 1500 m/s, the density is 2200 kg/m^3, $Q_p = 40$, and $Q_s = 20$. The model is discretized with 256×256 grid points. The grid spacing of the horizontal and vertical axes are $\Delta x = \Delta z = 6$ m. The source is at the origin point. Its center frequency is 25 Hz with a time delay of 0.04 s. The time step is 1 ms. The horizontal and vertical particle velocities are recorded through time with 400 receivers, which are located in a circle with radius 600 m centered at the source (Figure 2).

I generated synthetic viscoelastic data with a horizontal single force. Then I ran both elastic and viscoelastic back-propagation

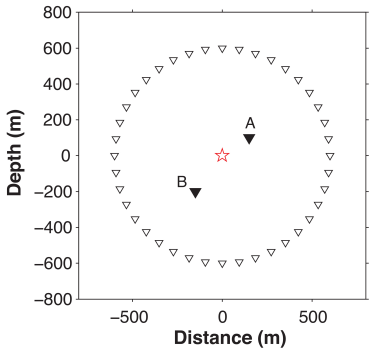

Figure 2: The source-receiver geometry for the first and second numerical experiments. The red star at the origin indicates the source. The open triangles indicate the receiver boundary. The filled triangles indicated two reference points. This example is in two dimensions. The coordinates of A and B are $(150, 100)$ m and $(-150, -200)$ m. Every tenth receiver is shown for clarity.

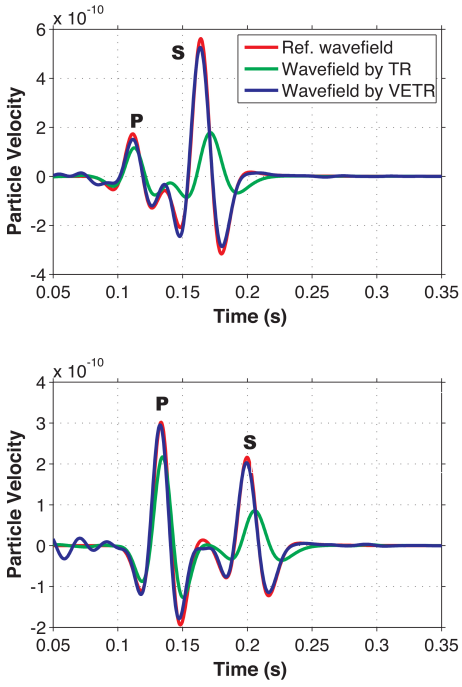

Figure 3: Waveforms (horizontal particle velocity component) recorded at the reference points A (top) and B (bottom). Red: waveform recorded in the forward simulation using viscoelastic forward modeling. Green: waveform reconstructed by elastic back-propagation. Blue: waveform reconstructed by viscoelastic back-propagation in this paper. The recovery of the waveform (blue) demonstrates that the equation for the viscoelastic back-propagation approach is time-invariant. The errors may be caused by the finite-difference discretization. Labels P and S denote P-wave and S-wave, respectively.

approaches. The Tukey filter was chosen with a cutoff frequency of 120 Hz and a taper ratio of 0.4. As a reference image, I also ran elastic back-propagation with simulated elastic data, i.e., without any attenuation effects.

In the first test, I show the time-invariance of the viscoelastic back propagation approach, i.e., that the waveform at a specified point in the computational grid can be reconstructed during viscoelastic back propagation propagation. Here I have two reference points A and B for all simulations in Figure 1.

Figure 3 shows reconstructed waveforms at reference points A and B. Due to attenuation between the reference points and receivers, the waveform reconstructed by elastic back-propagation (green line) is spread out (phase-shifted) and has reduced amplitude at both A and B compared to the reference waveform (red line). We can see that the more attenuated S-waves have larger shifts than the P-waves. Those incorrect waveforms at A and B reinforce that the attenuation breaks the time-invariance of time-reversal propagation. The reconstructed waveform by viscoelastic with attenuation compensation (blue line) is comparable to the reference waveform in amplitude and phase for both P- and S-waves. The recovery of the waveform demonstrates the time-invariance of the back-propagation equation for the viscoelastic.

The second model is the truncated Marmousi model. Figure 3a shows the quality factor Q in a 3×3 km region of the Marmousi model. For simplicity, the quality factor Q is defined as the square root of P-wave velocity. The model is discretized with 256×256 grid points. The grid spacing of the horizontal and vertical axes are $\Delta x = \Delta z = 12.5$ m. The red star represents a source at the location (0 300) m. Its center frequency is 20 Hz with a time delay of 0.04 s. The time step is $5.4e-4$ s. Two arbitrary reference points X_A and X_B are shown in the solid triangles. The open triangles denote a receiver line with 193 receivers. Every tenth receiver location is marked by an open triangle. The total time length of seismograms is 1.6 s.

In Figures 3b and 3c, the reference propagated waveforms at the X_A (top) and X_B (bottom) points in red are directly computed by viscoacoustic modeling from the source. The reconstructed Greens function using an acoustic time-reversal modeling method (green) and the viscoacoustic time-reversal modeling method (blue) are shown, respectively. Without attenuation compensation, there exits apparent difference in phase and amplitude compared to a reference solution (in red). With compensation, the good match in both amplitude and phase between the Green's functions computed by using the proposed method and the directly computed reference solutions, even at late times, are observed in Figs. 3b and 3c. These artifacts arrived before the primary waves are caused by scatterings after the arrivals of the primary waves during time-reversal propagation. If the receivers are fully sampled around the source (Fig. 3d), the primary waves show consistence between limited aperture (blue) and full aperture (black) receiver geometry but full aperture geometry obviously captures more information in coda waves (black lines in Figures 3e and 3f). The truncated waveforms in the subfigures emphasize the match in more detail.

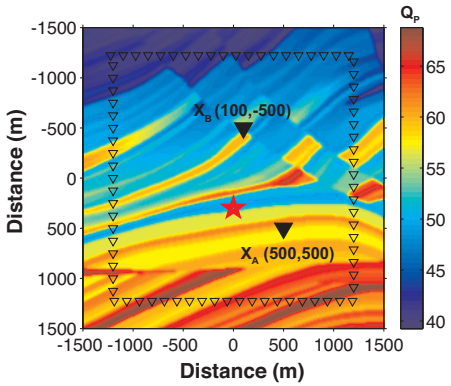

Figure 4: Marmousi heterogeneous Q_p model. The color scale indicates the P-wave quality factor. The model is bounded by absorbing boundary conditions on the four sides. The star represents a source. The two reference points X_A and X_B are used for comparison of waveforms. Every twentieth receiver on the surrounding surface S is marked by an open triangle.

Figure 5 presents the wavefield reconstruction results. When using viscoelastic back-propagation, the reconstructed waveform in the color green is corrected.

CONCLUSION

I presented wave propagation and wavefield reconstruction by back-propagation in viscoelastic media. With the analysis of decoupling attenuation operators in the viscoelastic wave equation, I demonstrated that either amplitude loss or velocity dispersion can be independently functioned on wave propagation. Further, the back propagation equation can be formulated by reversing the sign of both P- and S-wave loss operators while at the same time compensating for both P- and S-wave attenuation effects in the reconstructed wavefield and source. Numerical results show that the viscoelastic back-propagation approach is able to reconstruct the wavefield with the correct phase and amplitude at an arbitrary point in the media.

ACKNOWLEDGEMENTS

I would like to thank Jackson Postdoctoral Fellowship in the Jackson School of Geosciences at the University of Texas at Austin.

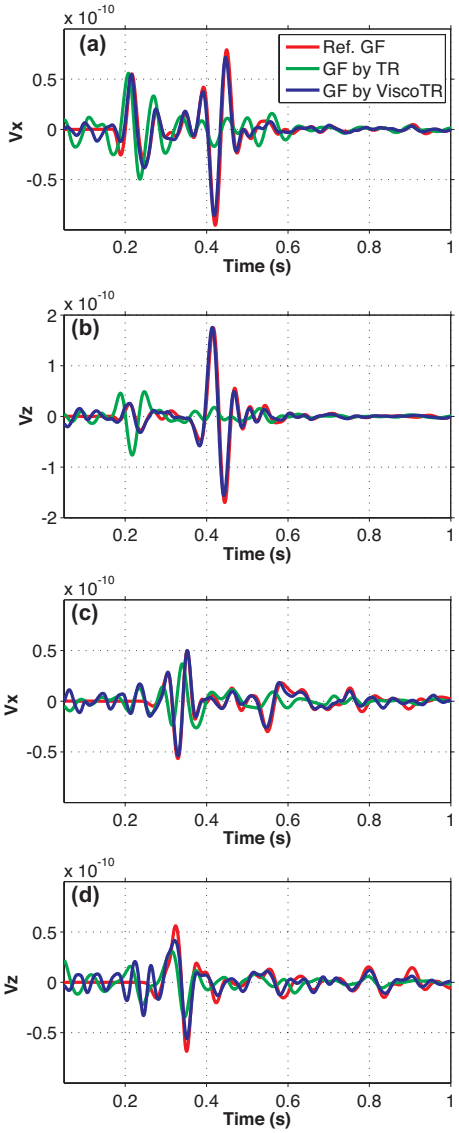

Figure 5: Reconstructed waveform and recorded at the reference points X_A (a,b) and X_B (c,d), respectively. The Vx and Vz components are reconstructed by elastic back-propagation (green) and by viscoelastic back-propagation (blue) compared to the reference solutions calculated by the viscoelastic forward modeling (red).

REFERENCES

Caputo, M., and F. Mainardi, 1971, A new dissipation model based on memory mechanism: Pure and Applied Geophysics, **91**, 134–147.

Carcione, J. M., 2009, Theory and modeling of constant-Q P- and S-waves using fractional time derivatives: Geophysics, **74**, T1–11.

Carcione, J. M., F. Cavallini, F. Mainardi, and A. Hanyga, 2002, Time-domain seismic modeling of constant-Q wave propagation using fractional derivatives: Pure and Applied Geophysics, **159**, 1719–1736.

Carcione, J. M., K. Helbig, and H. B. Helle, 2003, Effects of pressure and saturating uid on wave velocity and attenuation of anisotropic rocks: Int. J. Rock Mech. Min. Sci., **40**, 389–403.

Carcione, J. M., D. Kosloff, and R. Kosloff, 1988, Wave propagation simulation in a linear viscoelastic medium: Geophysical Journal, **95**, 597–611.

Dvorkin, J. P., and G. Mavko, 2006, Modeling attenuation in reservoir and nonreservior rock: The Leading Edge, **25**, 194–197.

Kjartansson, E., 1979, Constant-Q wave propagation and attenuation: Journal of Geophysical Research, **84**, 4737–4748.

McDonal, F. J., F. A. Angona, R. L. Mills, R. L. Sengbush, R. G. van Nostrand, and J. E. White, 1958, Attenuation of shear and compressional waves in pierre shale: Geophysics, **23**, 421–439.

Podlubny, I., 1999, Fractional Differential Equations: Academic Press.

Zhu, T., 2014, Time-reverse modelling of acoustic wave propagation in attenuating media: Geophysical Journal International, **197**, 483–494.

———, 2015, Viscoelastic time-reversal imaging: Geophysics, **80**, A45–A50.

Zhu, T., and J. M. Carcione, 2014, Theory and modelling of constant-q p- and s-waves using fractional spatial derivatives: Geophysical Journal International, **196**, 1787–1795.

Zhu, T., and J. M. Harris, 2014, Modeling acoustic wave propagation in heterogeneous attenuating media using decoupled fractional Laplacians: Geophysics, **79**, T105–T116.